Experimental consequences of quantum critical points at high temperatures

D. C. Freitas,[1,2] P. Rodière,[1] M. Núñez,[3] G. Garbarino,[4] A. Sulpice,[1] J. Marcus,[1] F. Gay,[1]
M. A. Continentino,[2] and M. Núñez-Regueiro[1,*]

[1]*Institut Néel, Université Grenoble Alpes & Centre national de la recherche scientifique (CNRS), 25 Av. des Martyrs, 38042 Grenoble, France*
[2]*Centro Brasileiro de Pesquisas Físicas, Rua Dr. Xavier Sigaud, 150, Rio de Janeiro, 22290-180, Brazil*
[3]*Consejo Nacional de Investigaciones Científicas y Técnicas, Buenos Aires, Argentina; Instituto de Ciencias Básicas, Universidad Nacional de Cuyo, Mendoza, Argentina; Departamento Materiales Nucleares, Centro Atómico Bariloche, Comisión Nacional de Energía Atómica, 8400 Bariloche, Argentina*
[4]*European Synchrotron Radiation Facility (ESRF), 6 Rue Jules Horowitz 38043 BP 220 Grenoble, France*

(Received 21 May 2014; revised manuscript received 15 September 2015; published 23 November 2015)

We study the $Cr_{1-x}Re_x$ phase diagram finding that its phase transition temperature towards an antiferromagnetic order T_N follows a quantum $[(x_c - x)/x_c]^{\psi}$ law, with $\psi = 1/2$, from the quantum critical point (QCP) at $x_c = 0.25$ up to $T_N \approx 600$ K. We compare this system to others in order to understand why this elemental material is affected by the QCP up to such unusually high temperatures. We determine a general criterion for the crossover, as a function of an external parameter such as concentration, from the region controlled solely by thermal fluctuations to that where quantum effects become observable. The properties of materials with low coherence lengths will thus be altered far away from the QCP.

DOI: 10.1103/PhysRevB.92.205123 PACS number(s): 75.30.Fv, 64.70.Tg

I. INTRODUCTION

Theoretical studies by Hertz [1] and Millis [2] (HM) have directed research towards quantum phase transitions [quantum critical points (QCPs)] [3,4] induced by an external parameter δ, such as doping, pressure, or magnetic field [5,6]. In thermal phase transitions, the critical temperature results from the competition between an interaction that drives the system to an ordered state and the entropy, which increases in the presence of thermal disorder. As QCPs occur at zero temperature, there is no entropy, and it is now the competition among the different terms of the Hamiltonian describing the material that gives rise to the QCP. In an itinerant magnetic system, this competition involves the Coulomb repulsion U between electrons and the electronic kinetic energy, as expressed by the bandwidth W. An increase of the ratio U/W due to pressure or doping can thus set up a magnetic ground state at a QCP. In three dimensions, this ground state is robust to thermal fluctuations and exists up to a critical temperature, which has a power law dependence with the distance to the QCP. Quantum critical points have been studied in heavy fermions [7], whose characteristic energies rarely exceed 30 K, and the present theory has successfully interpreted the main experimental results. On the other hand, although calculations on ideal systems have predicted observation of quantum critical behavior over an extended temperature range [8], experimental evidence is needed to support these theoretical predictions. Furthermore, few papers have addressed the passage from classical to quantum dominated regions of the phase diagram of elemental materials.

Chromium presents a spin density wave (SDW) due to the nesting of the hole and electron pockets of its Fermi surface that develops at a Néel temperature $T_N = 312$ K. The Cr metal displays two clearly defined regimes on its way to the QCP, both as a function of pressure P or vanadium doping x ($Cr_{1-x}V_x$). A classical region at low P or x, where T_N decreases following an exponential with pressure at a Bardeen-Cooper-Schrieffer (BCS tuned variation [9], is a consequence of the dependence of T_N with the coupling parameter λ, i.e., $T_N \sim e^{-1/\lambda}$. A quantum region appears below a crossover value [10,11] of T_N where quantum effects take control through a power law behavior with an exponent $\psi = 1/2$, which is the same for P and x .

Partial substitution of Cr by Re increases the electron count of the alloy. It first enhances the nesting and thus augments T_N; it then decreases it, and at $x \sim 0.15$, superconductivity appears [12], coexisting with antiferromagnetism. As metallurgical drawbacks cast doubts on these reported results, we have determined a detailed phase diagram with more homogenously sputtered samples of the $Cr_{1-x}Re_x$ system.

II. EXPERIMENTAL

The sputtered series of samples was grown using a magnetron sputtering apparatus with characteristics similar to those of Ref. [13], with a base pressure below 5×10^{-8} Torr. The Cr sputtering target was covered with appropriate angular portions of Re 0.2 mm foil to the desired concentration. The gun was powered with 150 W dc, and $Cr_{1-x}Re_x$ films were deposited at rates of 0.5–1.0 Å/s onto substrates of amorphous SiN_x/Si held at room temperature. The Ar sputtering gas pressure was approximately 0.75 mTorr. The Re concentration was verified by scanning electron microscope.

In bulk samples, it is difficult to avoid concentration gradients because of the high liquidus temperature of the alloys (above 2000 °C) together with the high vapor pressure of Cr at elevated temperatures [14]. This metallurgical drawback is amplified at higher Re concentrations (approximately $0.2 < x_{Re} < 0.3$), allowing phase separations, which can explain the coexistence of low Re content regions (having a $T_N \approx 157$ K) with high Re regions (superconducting with $T_{sc} \approx 2.7$ K) in the bulk samples. The sputtering technique circumvents these

*To whom correspondence should be addressed: manolo.nunez-regueiro@neel.grenoble.fr

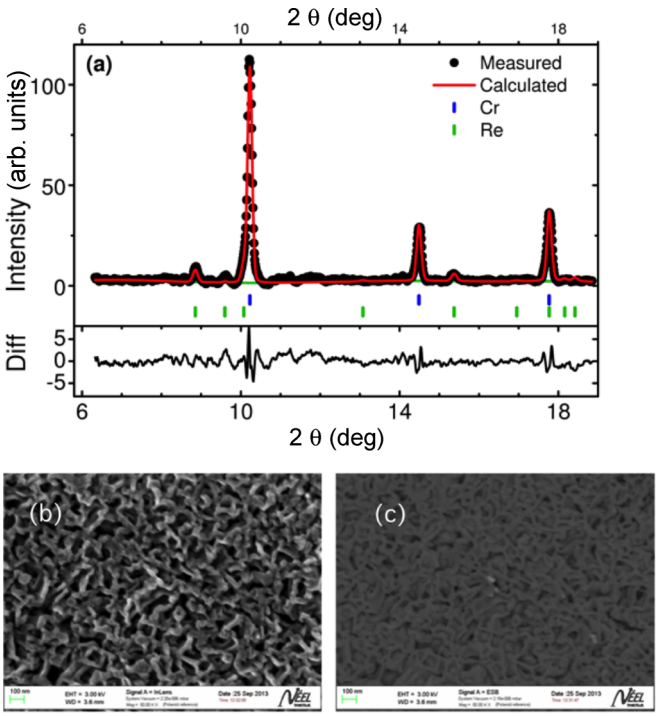

FIG. 1. (Color online) (a) Synchrotron x-ray diffraction pattern for the $x = 0.246$ sample. The Rietveld fit yields a 97 wt% of bcc Cr phase and only a 3 wt% of hexagonal Re, showing that the sample is mainly monophasic. (b) In-lens detector photograph of the surface showing the small crystallite size (∼30–100 nm). (c) Measurement of composition by electron backscattering detector. The white spots correspond to silver paint speckles. We observe a homogeneous distribution of Cr and Re. For this sample, the energy dispersive x-ray spectroscopy (EDX) analysis on five different spots gave a Re concentration of 0.187 ± 0.007. The black spots correspond to the SiN_x substrate.

metallurgical problems by creating a homogeneous plasma with the Cr/Re ratio of the target, which is then deposited at room temperature into a film with the corresponding homogeneity. The very quick annealing does not affect this initial homogeneity, as confirmed by our scanning electron microscope analysis and x-ray synchrotron measurements (Fig. 1).

The electrical resistivity was measured using a four lead direct current method. Depending on the temperature range, the contacts were tungsten fingers or platinum leads with silver epoxy. Annealing and high temperature electrical resistivity measurements were done simultaneously in a homemade optical furnace with the four tungsten fingers. The samples were heated up to 800 °C in a 10 minute lapse and measured down to room temperature at the same speed. Low temperature measurements were done on ^{3}He and ^{4}He cryostats. Magnetization measurements were performed down to 2 K in a Métronique Ingénierie superconducting quantum interference device (SQUID) (sensitivity 10^{-7} emu at low field and 10^{-5} emu at high field).

The angle dispersive x-ray diffraction studies on CrRe film samples were performed at the ID27 high-pressure beamline of the European Synchrotron Radiation Facility using monochromatic radiation ($\lambda = 0.3738$ Å). The diffraction patterns were collected with a charge-coupled device (CCD) camera, and the intensity vs 2θ patterns were obtained using the Fit2D software [15]. A complete Rietveld refinement was done with the GSAS-EXPGUI package [16].

For the *ab initio* calculation of the Fermi surfaces, we used density functional theory as implemented in the quantum ESPRESSO code [17], which uses a plane wave basis to describe the electronic wave functions and ultrasoft pseudopotentials to represent the interaction between electrons and ions [18]. The exchange and correlation potential was considered at the level of the generalized gradient approximation (GGA) based on the Perdew-Burke-Ernzerhof (PBE) expression [19]. A body-centered-cubic (bcc) I cell was used with one Cr atom. Reciprocal space integrations were performed on a (12 × 12 × 12) Monkhorst-Pack mesh [20]. The doping of Cr with Re was simulated by using a rigid band method by adding extra electrons inside the supercell. Therefore, the case of $Cr_{1-x}Re_x$ is calculated by adding a fraction X of an electron into the cell plus the adjustment of the lattice parameter to the correspondent experimental value. For all the different fractions X of electronic charge added in the supercell, we find that the experimental value $X = 0.02$ is reproduced in the calculations with $X = 0.2$. This difference can be adjusted with a scissors kind of method, as explained next.

The *ab initio* calculated electronic structure corresponds to the paramagnetic phase and anticipates the situation previous to the formation of a SDW. Three bands are involved at the Fermi level [21], one of them (the reservoir) with a high density of state (D) that is around 2.4 times the total density of states of the other two bands at H and Γ at their Fermi surfaces. Electrons are expected to flow from the reservoir to the other two bands during the process of formation of the SDW, thus elevating the Fermi level by certain quantity D_{Fermi}. We estimate this value and adjust accordingly the Fermi levels of the calculated band structures as an approximation of the complex dynamics involved. The Fermi level of the reservoir will be depressed by $n/2D$, with n being the number of electrons. We fix $n = 0.18$ as the difference between the experimental and calculated values and approximate $D_{\text{Fermi}} = 2.4\,n/2D$. The total density of states evaluated at the Fermi level can be expressed as $D_{\text{tot}} = 3.4 \times D$ and can be obtained from the *ab initio* calculations. With all these ingredients, a value of D_{Fermi} of 0.13 was obtained, and all the Fermi surfaces were adjusted accordingly.

III. RESULTS

In Fig. 2, we show the electrical resistances of the samples as a function of temperature. The characteristic anomaly due to the SDW is clearly seen on the resistivity curves. We determine the Néel temperature T_N by the peak of the temperature derivative of the resistance as usual and show in Fig. 3 the obtained values as a function of Re substitution together with other reported values [12,22]. Far from the QCP, our values agree with precedent reports. Beyond $x \approx 0.2$, we do not confirm a constant value for T_N. Contrary to previous papers [12,22] (triangles in Fig. 2), we do not observe coexistence between magnetism and superconductivity down to 400 mK. Above $x \approx 0.25$, the superconducting transition temperature T_{sc} increases monotonically. We do not observe a

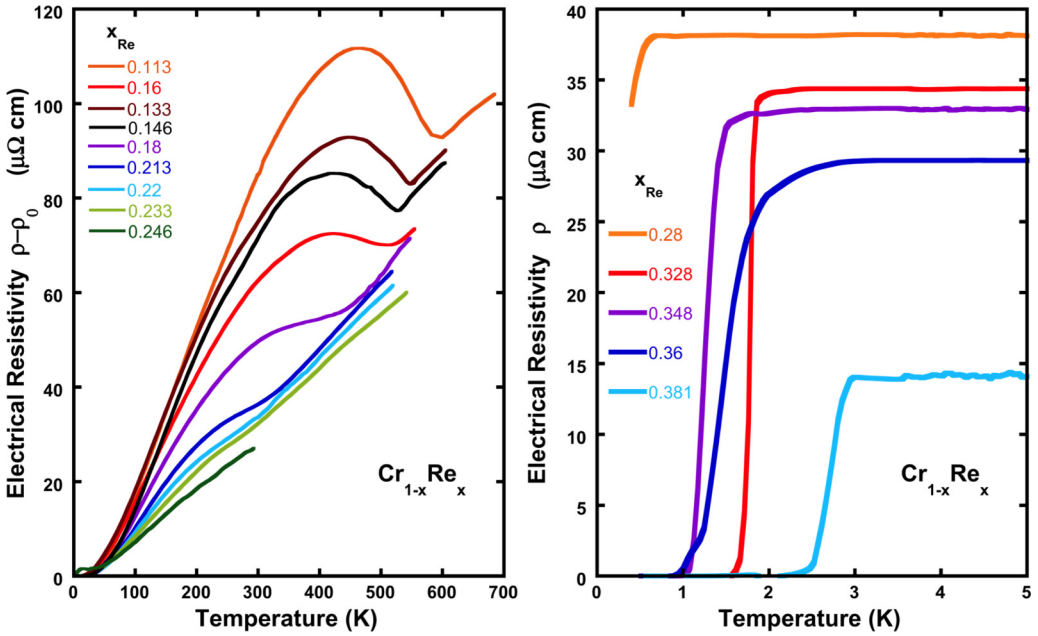

FIG. 2. (Color online) Electrical resistance for samples with different Re content. Left panel: High temperature behavior of the low concentration region (with residual resistivity subtracted). The $x = 0.246$ curve was obtained by cooling under magnetic field [see text and Fig. 3(d)]. The Néel temperature is defined by the steepest increment of the curves, as obtained from their derivative. Right panel: Low temperature, high concentration region, showing the superconducting transitions. The superconducting transition temperature is taken at the onset of the transition.

Meissner effect down to 2 K for samples with $x < 0.36$. As the precedents publications reported T_cs > 2 K down to concentrations $x \sim 0.2$, our SQUID measurements confirm our electrical resistivity results. The difference between our data and the published data is certainly due to the different sample homogeneity. It is clear from our results that superconductivity is quenched in the region where Cr is antiferromagnetic. Consequently, the observed superconductivity is presumably conventional electron-phonon superconductivity due to bcc Re, which is similar to that observed in W/Re and Mo/Re alloys [12]. The superconducting dome frequent at QCPs [7] is absent.

In most previously studied QCPs, the low temperature dependence of the resistivity yields a T^2 type term due to electron-electron correlations [7]. In our measurements, we observe for all concentrations an inelastic electron-phonon scattering Bloch-Grüneisen T^5 dependence [Fig. 3(a)], as has also been observed in epitaxial chromium films grown by a sputtering technique [13]. Something similar happens in pure bulk Cr [10] and Cr/V alloys [23], which have been shown to give a T^3 dependence, attributed in those reports to weakly inelastic electron-phonon scattering. We conclude that for chromium alloys, the electron-phonon coupling is the main source of carrier scattering. We also show in Fig. 3(b) the evolution with concentration of the residual resistivity. It is tempting to associate its behavior to the evolution of the antiferromagnetic gap. However, besides the existence of domains, it has been shown [13] that the residual resistivity of sputtered films can be strongly dependent on fabrication conditions precluding any reliable analysis.

In the measurements on chromium metal described in Ref. [10], besides obtaining near the QCP the $[(x_c - x)/x_c]^{\psi}$ law with $\psi = 1/2$, it was possible to obtain an exponent $\alpha = 1/4$ from the critical scaling of the inverse Hall coefficient and an exponent $\beta = 1/4$ from the scaling of $\Delta\rho/\rho$. In our $Cr_{1-x}Re_x$ samples, these scalings were impossible due to the following: The Hall coefficient for all our samples presents a change of sign at about 200 K; that change would necessitate a two-band analysis to do the inverse Hall constant scaling, removing any precision in the scaling [Fig. 3(c)].

On the other hand, our samples are polycrystalline and multidomain, the orientation of which will depend on the particular microstructure of each sample. Thus, in our case the amplitude of the transition will strongly depend on the domain structure, precluding any serious scaling analysis of $\Delta\rho/\rho$. It is known that cooling under a strong magnetic field orients the domains, forming a monodomain in monocrystals [24]. The amplification of the anomaly that results from a SDW wave vector $\boldsymbol{Q}$ parallel to the measuring current has helped us in determining the transitions for the samples whose Néel temperature was below 300 K, the maximal temperature at which we could apply a magnetic field. We show in Fig. 3(d) the example of the effect of cooling under a strong magnetic field for the nearest to critical concentration sample ($x = 0.246$).

We now search in the phase diagram of Fig. 4 for the classical and the quantum regimes obtained for Cr under pressure or V doping. The nonmonotonic behavior with doping and the incommensurate to commensurate SDW transition [22] at $x \approx 0.02$ make it difficult to define the classical exponential with doping regime at low Re doping. The quantum regime is clearly visible for doping concentrations above $x \approx 0.1$, as $T_N(x)$ follows a $[(x_c - x)/x_c]^{\psi}$ law with $\psi = 1/2$. Our measurements indicate that the quantum effects expected to be important only at low temperatures control the variation

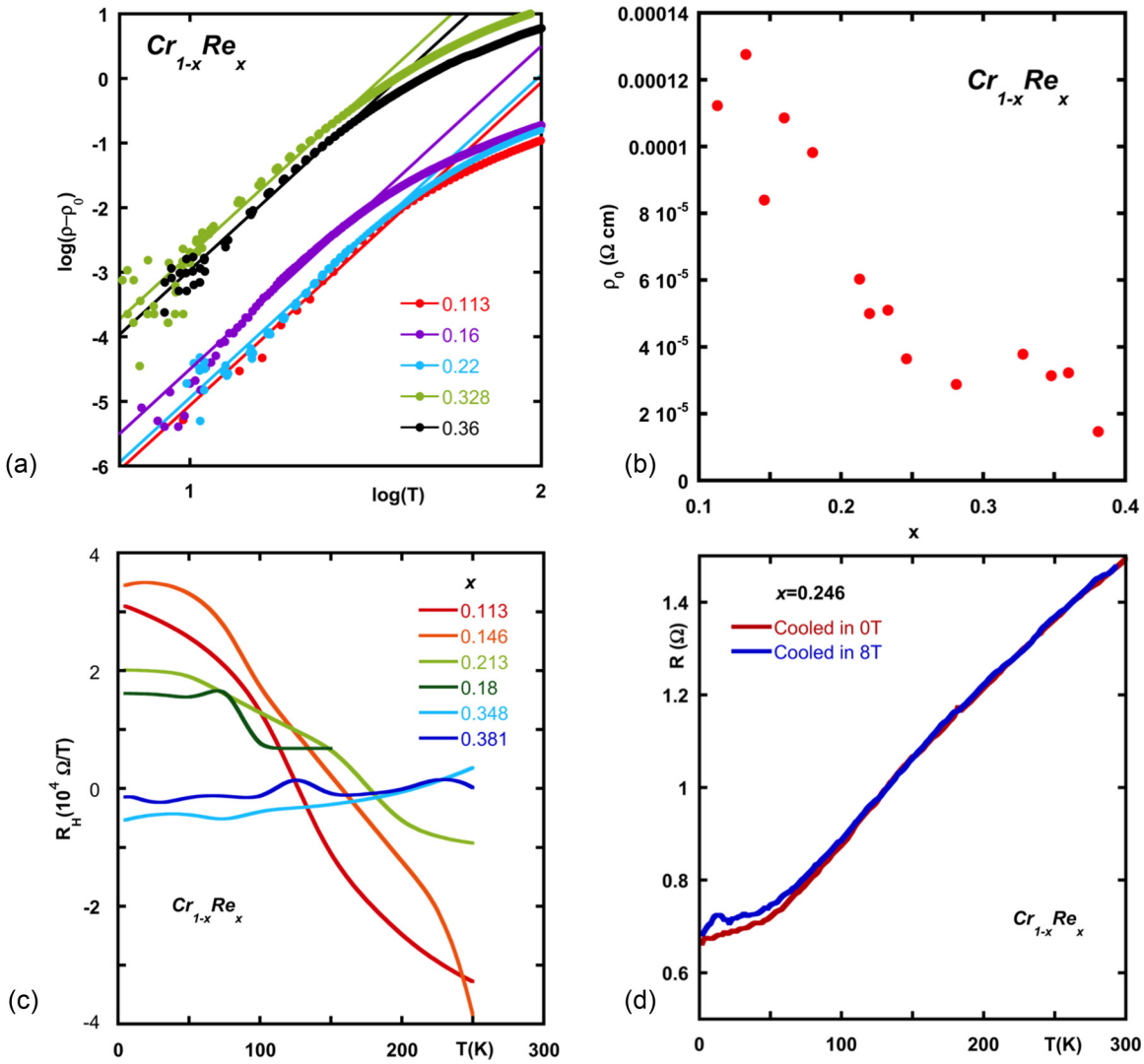

FIG. 3. (Color online) (a) Double logarithmic plot to show the T^5 temperature dependence (straight lines). (b) Residual resistivity as a function of concentration. (c) Hall constant as a function of temperature for several concentrations. (d) Evidence for antiferromagnetic domain ordering due to cooling under a magnetic field of 8 T from temperatures much higher than T_N for the sample nearest to the critical concentration.

of T_N from ∼600 K down to the QCP. We understand this as follows. The finite temperature transition at T_N is a classical critical phenomenon that arises in the renormalization group (RNG) approach. The RNG shows that a finite temperature fixed point always governs the critical behavior along the critical line, i.e., temperature is a relevant field at the QCP. For chromium and its alloys, the same parameters govern the phase diagram in the whole pressure range. However, while the BCS exponential behavior results from a competition with entropic effects, the power law behavior is a consequence of purely quantum effects. Then, as long as T_N depends on the distance to the QCP, its dependence is reflecting the competition between the quantum effects that gave rise to the QCP. In this sense, the power law behavior of T_N with the distance to the QCP is a direct evidence of quantum effects up to ∼600 K. Unfortunately, the study of criticality for other physical quantities, specifically, the Hall effect and increase of the resistance at T_N was impossible due to two-band effects and domains, respectively, as explained above.

IV. DISCUSSION

The free energy density, including quantum effects, within a mean field of a magnetic system that at $T = 0$ K will develop a QPT at an external parameter δ_c can be written

$$F = \tfrac{1}{2}\alpha(\delta - \delta_c)M^2 + \tfrac{1}{4}uM^4 + \tfrac{1}{2}\xi_{\mathrm{coh}}^2(\nabla M)^2, \qquad (1)$$

where M is the order parameter, ξ_{coh} is the coherence length, and α and u are constants. Temperature essentially introduces two corrections to the critical external parameter,

$$\delta_c^*(T) = \delta_c - bT^2 - uT^{1/\psi}.$$

The T^2 term arises from an analytic expansion of the free energy in powers of the temperature. A detailed analysis of the origin of the $1/2$ can be found for bosonic modes (phonons) in Ref. [25] and for fermionic modes in Ref. [26]. It is an analytic term that arises naturally from expansions of the Fermi-Dirac or Bose-Einstein statistics for particle-hole excitations in metals or for phonons in insulators, respectively.

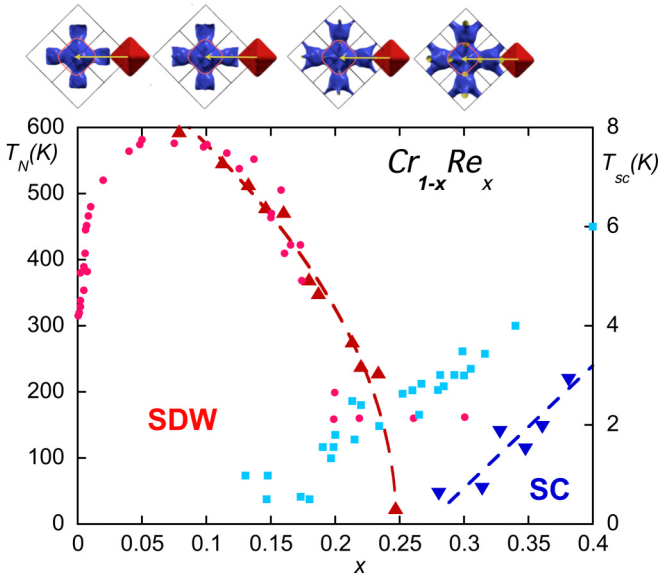

FIG. 4. (Color online) Lower panel: Phase diagram of $Cr_{1-x}Re_x$ as a function of Re content. Previous determinations of T_N are from Ref. [22] (mauve circles) compared to our data (red triangles). The previously reported superconducting transition temperatures (Ref. [12]) are shown (light blue squares) together with our data (blue inverted triangles). It is clear from the data for our more homogenous samples that superconductivity does not coexist with antiferromagnetism, precluding a nonconventional superconductor. We also observe that the decrease of T_N follows the power law $718[(0.248 - x)/0.248]^{0.5}$ from ~600 K down to the QCP. Upper panel: For illustration purposes, we show the Fermi surfaces of the Cr-Re alloy at $x = 0, 0.1, 0.2$, and 0.3 illustrating the nesting wave vector that changes from incommensurate (0) to commensurate (0.1; 0.2) and then back to incommensurate (0.3).

One general way of obtaining it is to consider a mean-field expansion of a Landau free energy for a quantum phase transition with order parameter M, say at a critical parameter δ_c. This is given by

$$F = \tfrac{1}{2}(\delta - \delta_c)M^2 + \tfrac{1}{4}uM^4.$$

Minimizing F with respect to M, we obtain

$$M \propto \sqrt{(\delta - \delta_c)}$$

as appropriate for a mean field theory.

Now we consider finite temperatures and write this free energy as

$$F(T) = \tfrac{1}{2}(\delta - \delta_c + T^2)M^2 + \tfrac{1}{4}uM^4,$$

which we rewrite as

$$F(T) = \tfrac{1}{2}\left(-T_N^2(\delta) + T^2\right)M^2 + \tfrac{1}{4}uM^4 \qquad (2)$$

with $T_N^2(\delta) = \delta - \delta_c$ or $T_N(\delta) = \sqrt{\delta - \delta_c}$.

Now we consider a fixed pressure and $T \to T_N(\delta)$, such that we can rewrite Eq. (2) as

$$F(T) = T_N(\delta)[T - T_N(\delta)]M^2 + \tfrac{1}{4}uM^4, \qquad (3)$$

which, when minimized with respect to M, yields the correct mean-field behavior

$$M \propto \sqrt{T_N(\delta) - T}.$$

Thus, with Eq. (3) for $T_N(\delta)$, we obtain the correct mean-field result for the finite temperature transition also.

The mean-field result is always present regardless of the character, fermionic or bosonic, of the critical modes close to the QPT. It is also independent of the universality class of the transition and does not convey any information on the nature of the QPT. The energy/time HM treatment yields the nonanalytic term $T^{1/\psi}$, which is due to the quartic interaction (uM^4) [4] that is dangerously irrelevant for systems with effective dimensions $d + z > d_{\text{eff}}$, where $d_{\text{eff}} = 4$ for magnetic transitions. Here, z is the dynamic exponent that takes the value $z = 2$ for a nearly antiferromagnetic metal, and d is the dimensionality. The shift exponent that depends on the universality class of the quantum phase transition can be expressed in terms of these later quantities as $\psi = (d + z - 2)/z$. Then, for an itinerant system in $3d$ near an antiferromagnetic QCP, we expect $\psi = 3/2$ so that at sufficiently low temperatures it always determines the shape of the critical line. However, as $\frac{1}{\psi} < 2$, this may occur only at very low temperatures, especially if the quartic interaction u is very small. For chromium alloys (and the cases that will be discussed below), the analytic T^2 term seems to be always the dominant one. Furthermore, the range in temperature of the validity of this law gives strong evidence that its origin is as discussed above and not from unknown fluctuations with dynamic exponent $z = 1$, which in $3d$ leads to $\psi = 1/2$.

However, what makes the transition towards the SDW in $Cr_{1-x}Re_x$ already under the influence of the QCP at such high temperatures? The answer is inherent in the third term of Eq. (1), implying that systems with large coherence lengths will be harder to deform and are presumably less sensitive to quantum effects, a hypothesis that is supported by the following facts.

The range of observation of the square root power law varies from $T_N \sim 60$ K for pure chromium to $T_N \sim 600$ K for $Cr_{1-x}Re_x$ alloys, suggesting that an increase of disorder causes the observation of quantum effects at higher temperatures. There are at least two other compounds that show a behavior with pressure similar to that of Cr metal. The one-dimensional transition metal trichalcogenide $NbSe_3$, a well-studied charge density wave (CDW) compound [27–29] and $\beta - Na_{0.33}V_2O_5$, a material with a charge order (CO) [30]. As shown on the left panel of Fig. 3, at low pressures these compounds follow the classical exponential with pressure dependence. At a certain value (different for each material) of the transition temperature—$T_{\text{CDW}} \sim 90$ K for $NbSe_3$, $T_{\text{CO}} \sim 30$ K for $\beta - Na_{0.33}V_2O_5$, and $T_N \sim 60$ K for Cr—the quantum regime sets in.

The above described conventional behavior contrasts with the one shown by the four materials on the right panel of Fig. 5. Layered 1T-$TiSe_2$ develops a CDW, thought to be the result of a transition towards an excitonic insulator at 200 K at ambient pressure [31]. One-dimensional orthorhombic (o)-TaS_3 develops a CDW at 215 K at ambient pressure [32] and the layered high temperature superconducting pnictide $BaFe_2As_2$ an antiferromagnetic ordering at 135 K at ambient pressure [33]. All three follow the $[(P_c - P)/P_c]^{0.5}$ law in the entire pressure phase diagram, as does $Cr_{1-x}Re_x$ as a function of concentration.

The simplest quantity that sorts the materials into the corresponding class is the measured zero temperature

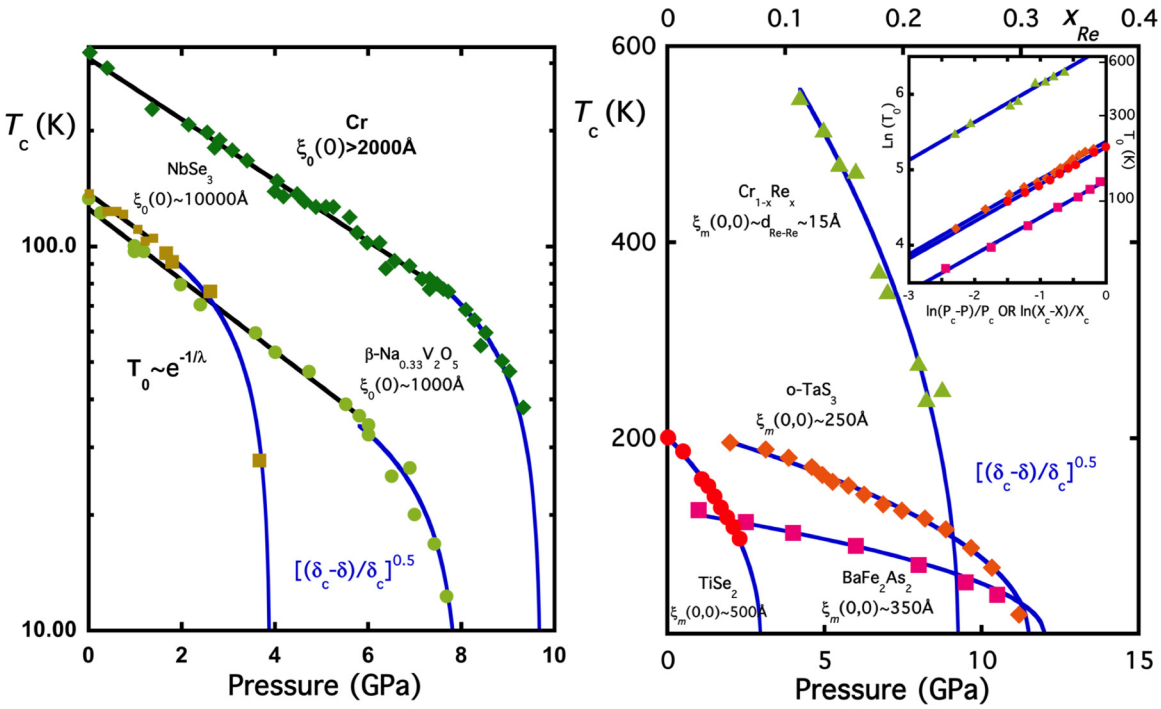

FIG. 5. (Color online) Left panel: Evolution of the ordering transition temperatures for different materials showing an exponential decrease with pressure of the ordering temperature at low pressures (black lines), followed at high pressures by the $[(P_c - P)/P_c]^{0.5}$ law (blue lines). $\beta - Na_{0.33}V_2O_5$ (light green circles) (Ref. [30]); $NbSe_3$ (light brown squares) (Ref. [28]); and Cr (green diamonds) (Ref. [9]). Right panel: Materials that show the $[(\delta_c - \delta)/\delta_c]^{1/2}$ (δ is either pressure or concentration) law in all the measured range. Inset: Log-log plot to obtain the power of the $[(\delta_c - \delta)/\delta_c]^{\psi}$; the slopes of the blue lines give a value of ψ for 0.50, 0.49, 0.49, and 0.50 for o-TaS_3 (orange diamonds) (Ref. [32]), 1T-$TiSe_2$ (red circles) (Ref. [31]), $BaFe_2As_2$ (mauve squares) (Ref. [33]), and $Cr_{1-x}Re_x$ (light green triangles), respectively. This type of fit yields a very reliable value of the exponent. For the measured zero temperature coherence lengths at ambient pressure or zero concentration ξ_{meas}, see the text and Table I.

coherence length at ambient pressure or zero concentration ξ_{meas}, either experimentally obtained or estimated from domain size (Table I). In $NbSe_3$, both from x-ray measurements [34] or nonlinear conductance [35] (that yield the depinning domains), at low temperatures the correlation length has a very large size, ~10 000 Å, while a lower limit [36] for domains in $\beta - Na_{0.33}V_2O_5$ is 1000 Å; however, the correlation length [37], as measured by x-ray diffraction at 5 K in Cr, is well over 2000 Å. In contrast to $NbSe_3$, for o-TaS_3 the correlation length can be roughly estimated from x-ray measurements [38] at about 500 Å. Different chirality [39] renders domains of ~500 Å in 1T-$TiSe_2$, while the measured magnetic correlation length [40] of $BaFe_2As_2$ at 3 K is ~350 Å. Finally, a crude lower estimate for $Cr_{1-x}Re_x$ in our measurement range can be given by the distance between Re atoms, ~15 Å; as we are in the dirty limit, the domain coherence length will certainly be limited by the impurities (Re atoms) in this case.

The compounds on the left panel of Fig. 5 have all $\xi_{meas} \geqslant 1000$ Å, while the materials on the right panel have all $\xi_{meas} \leqslant 500$ Å. Consequently, quantum effects dominate the entire phase diagram of materials with small correlation lengths, either intrinsic or impurity controlled. This argument can be quantified further through a simple calculation, showed graphically in Fig. 6.

There are two regimes, classical and quantum, and we want to determine when the system crosses over from one to the other. For the classical regime, the transition temperature is, according to BCS, $T_c^{class} = \hbar\omega_0 e^{-1/\lambda}$, where ω_0 is a characteristic energy and λ is the coupling parameter. The BCS coherence length is $\xi_{coh} = v_F/\Delta$, where v_F is the velocity at

TABLE I. Measured coherence lengths and estimation method.

Compounds	Coherence Length $\xi_m(0,0)$Å	Method	Reference
Cr	2000	x-ray diffraction	38
$NbSe_3$	10 000	x-ray diffraction	35
$\beta - Na_{0.33}V_2O_5$	1000	x-ray diffraction	37
o-TaS_3	500	x-ray diffraction	39
1T-$TiSe_2$	500	scanning tunneling microscopy	40
$BaFe_2As_2$	350	neutron diffraction	41
$Cr_{1-x}Re_x$	15	estimated impurity	

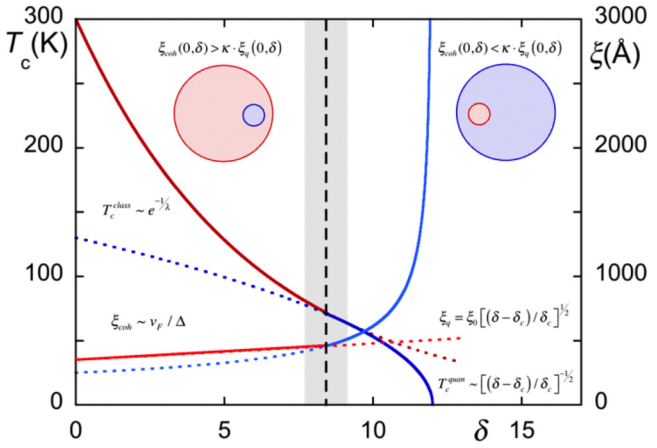

FIG. 6. (Color online) Schematic phase diagram showing the behavior of a typical ordering transition as a function of an external parameter δ. The crossover from the BCS exponential to the quantum power law regime is governed by a crossover ratio κ (unity in the figure) of the zero temperature intrinsic correlation length $\xi_{\rm coh}(0,\delta)$ to the quantum correlation length $\xi_q(0,\delta)$.

the Fermi level, and Δ is the BCS gap, proportional to $T_c^{\rm class}$. For the quantum regime, the transition temperature is given by $T_c^{\rm quan} = T_{c0}^{\rm quan}[(\delta_c - \delta)/\delta_c]^{1/2}$, while the quantum correlation length is $\xi_q = \xi_0[(\delta_c - \delta)/\delta_c]^{-1/2}$. The system changes regime when $T_c^{\rm quan} = T_c^{\rm class}$, thus the crossover occurs when the ratio $\frac{\xi_{\rm coh}}{\xi_q} = \kappa$, a constant particular to the system. Hence, materials with a small coherence length will be more affected by quantum fluctuations.

V. CONCLUSIONS

In summary, we have shown that the phase diagram of the $Cr_{1-x}Re_x$ system is controlled by the QCP up to temperatures $\sim$600 K. In terms of scaled temperatures, studies in heavy-fermion quantum criticality have shown that the quantum critical regime covers an entropy of about 50% of Rln2. On the other hand, the predictions for complex cuprates may also include high temperatures [8]. However, the fact that quantum effects take place already at such high actual, and not scaled, temperatures in elemental and noncomplex chromium is remarkable and unexpected. Finally, we have found evidence that suggests that the QCP can determine the state of the system for materials with small intrinsic coherence lengths far away from it not only in the δ coordinate but also in temperature T.

ACKNOWLEDGMENTS

D.C.F. gratefully acknowledges support from the Brazilian agencies CAPES and CNPq through grants CAPES BEX 0152/11-0 and CNPq 202353/2011-7. M.A.C. thanks the Brazilian Agencies CNPq grant 303298/2010-3 and FAPERJ grant E-26/201.370/2014. M.A.C. and M.N-R. acknowledge support from the grant CAPES-COFECUB Ph664/10. MN-R acknowledges A. Cano for discussions and S. Tanda for unpublished data. S. Pairis, B. Fernandez, P. Plaindoux, G. Giriat, and Th. Fournier have provided essential technical help.

[1] J. A. Hertz, Phys. Rev. B **14**, 1165 (1976).
[2] A. J. Millis, Phys. Rev. B **48**, 7183 (1993).
[3] S. Sachdev, *Quantum Phase Transitions* (Cambridge University Press, Cambridge, 1999).
[4] M. A. Continentino, *Quantum Scaling in Many-Body Physics* (World Scientific, Singapore, 2001).
[5] S. L. Sondhi, S. M. Girvin, J. P. Carini, and D. Shahar, Rev. Mod. Phys. **69**, 315 (1997).
[6] M. Vojta, Rep. Prog. Phys. **66**, 2069 (2003).
[7] H. von Löhneysen, A. Rosch, M. Vojta, and P. Wölfle, Rev. Mod. Phys. **79**, 1015 (2007).
[8] A. Kopp and S. Chakravarty, Nature Phys. **1**, 53 (2005).
[9] R. Jaramillo, Y. Feng, J. C. Lang, Z. Islam, G. Srajer, P. B. Littlewood, D. B. McWhan, and T. F. Rosenbaum, Nature **459**, 405 (2009).
[10] R. Jaramillo, Y. Feng, J. Wang, and T. F. Rosenbaum, PNAS **107**, 13631 (2010).
[11] Y. Feng, R. Jaramillo, G. Srajer, J. C. Lang, Z. Islam, M. S. Somayazulu, O. G. Shpyrko, J. J. Pluth, H.-K. Mao, E. D. Isaacs, G. Aeppli, and T. F. Rosenbaum, Phys. Rev. Lett. **99**, 137201 (2007).
[12] Y. Nishikara, Y. Yamaguchi, T. Kohara, and M. Tokomuto, Phys. Rev. B **31**, 5775 (1985).
[13] Z. Boekelheide, D. W. Cooke, E. Helgren, and F. Hellman, Phys. Rev. B **80**, 134426 (2009).
[14] J. Muheim and J. Müller, J. Phys. Kondens. Materie **2**, 377 (1964).
[15] A. P. Hammersley, S. O. Svensson, M. Hanfland, A. N. Fitch, and D. Hausermann, High Pressure Res. **14**, 235 (1996).
[16] B. H. Toby, J. Appl. Cryst. **34**, 210 (2001).
[17] P. Giannozzi, S. Baroni, N. Bonini, M. Calandra, R. Car, C. Cavazzoni, D. Ceresoli, G. L. Chiarotti, M. Cococcioni, I. Dabo, A. Dal Corso, S. de Gironcoli, S. Fabris, G. Fratesi, R. Gebauer, U. Gerstmann, G. Gougoussis, A. Kokalj, M. Lazzeri, L. Martin-Samos *et al.*, J. Phys.: Condens. Matter **21**, 395502 (2009).
[18] D. Vanderbilt, Phys. Rev. B **41**, 7892 (1990).
[19] J. P. Perdew, K. Burke, and M. Ernzerhof, Phys. Rev. Lett. **77**, 3865 (1996).
[20] H. J. Monkhorst and J. D. Pack, Phys. Rev. B **13**, 5188 (1976).
[21] A. Shibatani, K. Motizuki, and T. Nagamiya, Phys. Rev. **177**, 984 (1969).
[22] E. Fawcett, H. L. Alberts, V. Yu. Galkin, D. R. Noakes, and J. V. Yakhmi, Rev. Mod. Phys. **66**, 25 (1994).
[23] A. Yeh, Y.-A. Soh, J. Brooke, G. Aeppli, T. F. Rosenbaum, and S. M. Hayden, Nature **419**, 459 (2002).
[24] W. B. Muir and J. O. Ström-Olsen, Phys. Rev. B **4**, 988 (1971).
[25] A. Cano and A. P. Levanyuk, J. Supercon. Novel Mag. **19**, 417 (2006).
[26] T. Moriya, *Spin Fluctuations in Itinerant Electron Magnetism* (Springer Verlag, Berlin, 1985).
[27] M. Ido, Y. Okayama, T. Ijiri, and Y. Okajima, J. Phys. Soc. Jpn. **59**, 1341 (1990).
[28] M. Núñez-Regueiro, J.-M. Mignot, and D. Castello, Europhys. Lett. **18**, 53 (1992).

[29] S. Yasuzuka, K. Murata, T. Fujimoto, M. Shimotori, and K. Yamaya, J. Phys. Soc. Jpn. **74**, 1782 (2005).
[30] T. Yamauchi and Y. Ueda, Phys. Rev. B **77**, 104529 (2008).
[31] A. F. Kusmartseva, B. Sipos, H. Berger, L. Forró, and E. Tutis, Phys. Rev. Lett. **103**, 236401 (2009).
[32] M. Monteverde, J. Lorenzana, P. Monceau, and M. Núñez-Regueiro, Phys. Rev. B **88**, 180504(R) (2013).
[33] T. Yamazaki, N. Takeshita, R. Kobayashi, H. Fukazawa, Y. Kohori, K. Kihou, C.-H. Lee, H. Kito, A. Iyo, and H. Eisaki, Phys. Rev. B **81**, 224511 (2010).
[34] D. DiCarlo, R. E. Thorne, E. Sweetland, M. Sutton, and J. D. Brock, Phys. Rev. B **50**, 8288 (1994).
[35] J. McCarten, D. A. DiCarlo, M. P. Maher, T. L. Adelman, and R. E. Thorne, Phys. Rev. B **46**, 4456 (1992).
[36] S. Sirbu, T. Yamauchi, Y. Ueda, and P. H. M. van Loosdrecht, Eur. Phys. J. **B53**, 289 (2006).
[37] R. Jaramillo, Y. Feng, and T. F. Rosenbaum, J. Appl. Phys. **107**, 09E116 (2010).
[38] K. Inagaki, M. Tsubota, K. Higashima, K. Ichimura, S. Tanda, K. Yamanoto, N. Hanasaki, N. Ikeda, Y. Nogami, T. Ito, and H. Tokoyama, J. Phys. Soc. Japan **77**, 093708 (2008).
[39] J. Ishioka, Y. H. Liu, K. Shimatake, T. Kurosawa, K. Ichimura, Y. Toda, M. Oda, and S. Tanda, Phys. Rev. Lett. **105**, 176401 (2010).
[40] S. D. Wilson, Z. Yamani, C. R. Rotundu, B. Freelon, E. Bourret-Courchesne, and R. J. Birgeneau, Phys. Rev. B **79**, 184519 (2009).